SCIENCE CHINA
Chemistry

•REVIEWS•
SPECIAL ISSUE: Celebrating the 100th Anniversary of Chemical Sciences in Nanjing University

May 2020 Vol.63 No.5: 665–681
https://doi.org/10.1007/s11426-020-9748-0

Mesostructured carbon-based nanocages: an advanced platform for energy chemistry

Qiang Wu, Lijun Yang, Xizhang Wang & Zheng Hu*

Key Laboratory of Mesoscopic Chemistry of Ministry of Education, School of Chemistry and Chemical Engineering, Nanjing University, Nanjing 210023, China

Received January 8, 2020; accepted April 15, 2020; published online April 22, 2020

The electrochemistry in energy conversion and storage (ECS) not only relies on the active species in catalysts or energy-storage materials, but also involves mass/ion transport around the active species and electron transfer to the external circuit. To realize high-rate ECS process, new architectures for catalysts or energy-storage electrodes are required to ensure more efficient mass/charge transport. 3D porous mesostructured materials constructed by nanoscale functional units can form a continuous conductive network for electron transfer and an interconnected multiscale pores for mass/ion transport while maintaining the high surface area, showing great promise in boosting the ECS process. In this review, we summarize the recent progress on the design, construction and applications of 3D mesostructured carbon-based nanocages for ECS. The role of the hierarchical architectures to the high rate performance is discussed to highlight the merits of the mesostructured materials. The perspective on future opportunities and challenges is also outlined for deepening and extending the related studies and applications.

carbon-based nanocages, mesostructures, energy conversion and storage, enhanced mass/charge transport, multifunction platform

Citation: Wu Q, Yang L, Wang X, Hu Z. Mesostructured carbon-based nanocages: an advanced platform for energy chemistry. *Sci China Chem*, 2020, 63: 665–681, https://doi.org/10.1007/s11426-020-9748-0

1 Introduction

The mission for sustainable development of modern society has motivated intense exploration of clean renewable energies. In view of the intermittent characteristics of the renewable energies, usually there are two ways for their efficient utilization, *i.e.*, being stored in electrochemical energy storage (EES) devices, or driving energy conversion reactions to produce value-added fuels/chemicals [1–3]. The steady electric energy is then obtained by discharging the EES devices or oxidizing the fuels electrochemically in fuel cells. The heart of such energy conversion and storage (ECS) technologies lies in the efficient catalysts and energy storage materials. Achieving the high current density at low overpotential for catalysts and/or the combined high power and energy densities for energy storage materials is the key issues for practical applications [2,3].

In principle, the electrochemical ECS processes involve the coupled electron transfer with ion transport/diffusion to the active sites. The ideal electrode materials should possess high conductivity, large accessible surface area, and facilitated electrolyte penetration/wettability simultaneously [3,4]. Nanostructuring has long been adopted to improve the electrochemical properties of electrode materials due to the increased specific surface area (SSA), enriched defective sites and shortened ion solid-state diffusion length (if there is) [4,5]. Due to the abundant morphologies, tunable surface/electron structures, high intrinsic conductivity and excellent stability, the carbon-based nanostructures such as fullerene, nanotubes, graphene, graphdiyne and nancages have the

*Corresponding author (email: zhenghu@nju.edu.cn)

© Science China Press and Springer-Verlag GmbH Germany, part of Springer Nature 2020

great potential in energy chemistry [6–10], each of which has its merits and limitations. Among them, carbon-based nanocages, also named as hollow (nano)spheres or nanocapsules sometimes, feature the accessible large interior cavities with subnanometer microchannels across the shells, high SSA with abundant topological defects on the outer surface, and tunable electronic structures by easy doping of heteroatoms, and are becoming the multifunctional platform for energy applications [10,11]. Usually, the discrete nanocarbons tend to aggregate/restack when they are made into electrodes, leading to the low porosity and inferior mass/ion transport kinetics thereof. Thus, a large part of active sites could be unreachable, much deteriorating the ECS performances [12,13]. In recent years, the nanomaterial synthesis is experiencing a profound evolution from the empirical science ("cook-and-look") to prediction, design and controllable synthesis, and meanwhile, more and more research attention has shifted from individual nanosized materials to mesostructured ones, which often means multiscale, multicomponent and multifunction [14,15]. The assembly of nanoscale units (and/or macromolecules) into 3D porous mesostructures with a certain order has aroused intensive interest. Such 3D hierarchical architectures with the large SSA enable more active sites, the fully interconnected hierarchical porosity for ion transport, and the continuous conductive scaffold for electron transfer as schemed in Figure 1, which are desirable for realizing the full potential of all electrode materials and for achieving high-rate ECS process [3,16–20].

Different from the 'star' nanocarbons such as fullerene, nanotubes and graphene with thousands of publications each year, the carbon-based nanocages have not attracted wide attention for quite a long time until very recent years, as shown in Figure 2. Actually, the cage-like nanocarbons are the product of the same times of fullerene and nanotubes [21,22], usually appearing as the side product in preparing fullerene/nanotubes by arc discharge of graphite electrodes or prepared in the similar way, often with the encapsulated metals or metal carbides [23–26]. However, such nanostructures received little attention due to the low productivity and the difficulty for purification and applications [27]. The individual hollow nanocages were prepared by using silicon colloids as templates in 2002. The tin-filled carbon nanocages were firstly used as anode materials for lithium-ion batteries (LIBs) in 2003, and the carbon nanocages were used as supports for catalysts in 2004, which initiated the study of energy chemistry for the carbon-based nanocages [28–30]. Since 2012, thanks to the innovation of preparation methods and composite structures, the carbon-based nanocages could be conveniently prepared and regulated for various applications, leading to the rapid increase of related studies especially in energy chemistry [10,13,20,31–33]. In particular, the 3D mesostructures assembled from the carbon-based nanocage units possess the hierarchical architecture and interconnected micro-, meso- and macropores, which combines the accessible large interior cavities, the facilitated mass/charge transportation and the high SSA. Accordingly, such 3D mesostructures show great potential in accelerating the ECS process, becoming an advanced platform for energy chemistry beyond the individual nanocages [13,32–43]. In this review, we summarize the recent progress on the design, construction and applications of 3D mesostructured carbon-based nanocages for ECS. The role of mesostructures to the high rate performance is discussed to highlight their merits. The perspective on future opportunities and challenges is also outlined for deepening and extending the related studies and applications.

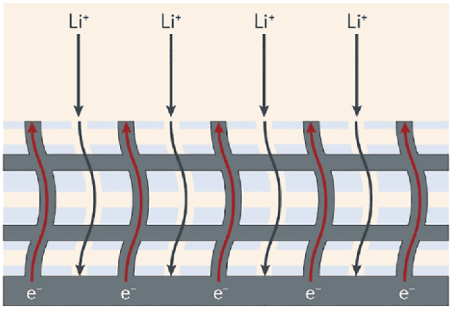

Figure 1 The 3D mesostructured electrode combining the large SSA, the fully interconnected hierarchical porosity, and the continuous conductive scaffold. Such an architecture is favorable for efficient charge delivery throughout the entire electrode [3] (color online).

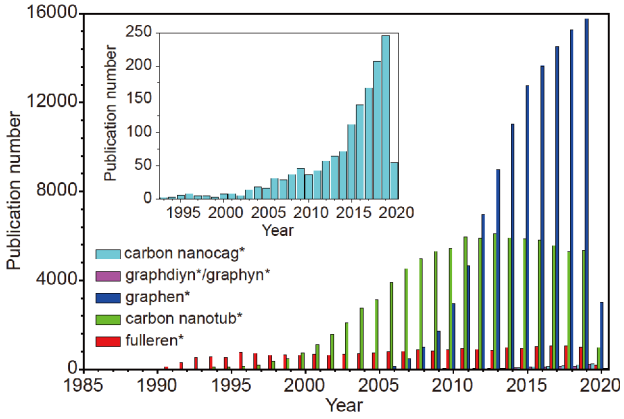

Figure 2 Publications each year for typical nanocarbons searched by Web of Science with keywords in TITLE. Inset shows the data for carbon nanocag* or carbon hollow spher* or carbon hollow nanospher* or carbon nanocapsul* (up to March 27 2020) (color online).

2 Mesostructured carbon-based nanocages

Nanostructuring electrode materials can increase SSA, enrich defective sites and shorten ion solid-state diffusion distance, beneficial to the utilization in ECS [4]. However, in

some cases, the aggregation/stacking of nanomaterials will lead to the poor electrolyte penetration to the surface of each unit, so that the effective active area of nanostructured electrodes is not as large as expected. Constructing 3D porous mesostructured electrodes can avoid such obstacles, showing great promise in energy chemistry.

2.1 Mesostructured materials

Mesostructured materials are usually a kind of complexes assembled by the nanoscale functional units with a certain ordered manner as schemed in Figure 3. The functional units contain the active sites while the porous peripheral architecture acts as the mass transport channels to the active sites. Mesostructure often means the multiscale, multicomponent and multifunction, leading to the new performance and applications (Figure 3(a)). In energy chemistry, the mesostructured materials not only have the advantages of large SSA and short ion diffusion distance due to the nanostructured units, but also demonstrate new collective properties favorable for rapid ECS process, *i.e.*, the smooth mass transport and electron transfer due to the interconnected pores and continuous conductive scaffold (Figure 3(b)).

The development of nanoscience and nanotechnology has accumulated a wealth of scientific knowledge and experimental skills, providing a foundation for studying the mesostructured materials. The invention of new synthetic methods and controllable construction of mesostructured materials, as well as the exploration of their interactions, functions and applications have attracted increasing attention in recent years [14,15]. The related research will much help address the major demands such as the efficient utilization of energy and resource, protection of environment and production of high-value chemicals.

To elucidate the expedience of mesostructured electrodes for charge/mass transfer through electrolytes, the diffusion of Li^+ ions within the 3D mesostructured electrodes was simulated by the finite element method (FEM). The size of the multiscale pores was turned into the inter-distance (d) of the electrode sheets (Figure 3(c)). The simulation results showed that the steady-state reaction current density (j) increases with increasing d value, accompanied by the increasing Li^+ ion concentration around the electrode sheets, which indicates the great significance of the mesostructured electrodes to achieve fast ion transfer and the high-rate ECS thereof (Figure 3(d)) [13].

2.2 Design and construction of mesostructured carbon-based nanocages

Templating method is a general approach to the hollow carbon nanocages, among which MgO template has been widely adopted because of the abundant sources, simple removal, low pollution and less interference to performances [10]. According to the morphology-inherited characteristics of the templating method, the mesostructured MgO template is the precondition to obtain the similar mesostructures of carbon nanocages as demonstrated in Figure 4. The mesostructured basic magnesium carbonate was prepared by a simple precipitation method: the aqueous solutions of $MgCl_2$ and Na_2CO_3 (0.2 M) was prepared respectively, and then quickly mixed under stirring. The mesostructured microspheres of basic magnesium carbonate tetrahydrate were then obtained by refluxing for appropriate time without stirring. The porous microspheres are composed of radially aligned nanosheets with a certain inter-sheet distance. The mesostructured basic magnesium carbonate was heated to 700–1,000°C under Ar flow in a tubular furnace, followed by

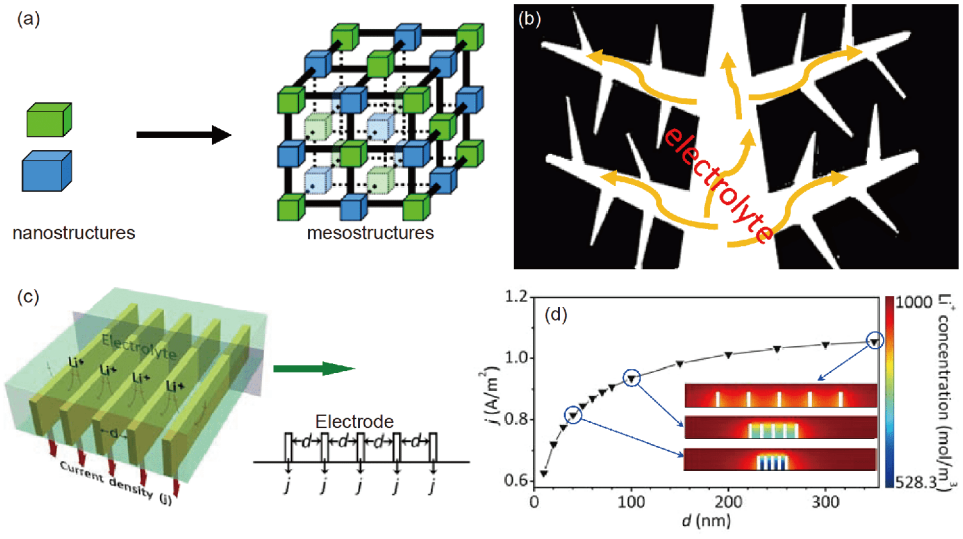

Figure 3 Schematic mesostructures with interconnected pores and continuous conductive scaffold for the smooth mass/charge transfer (a, b), and the FEM simulation results (c, d) [13] (color online).

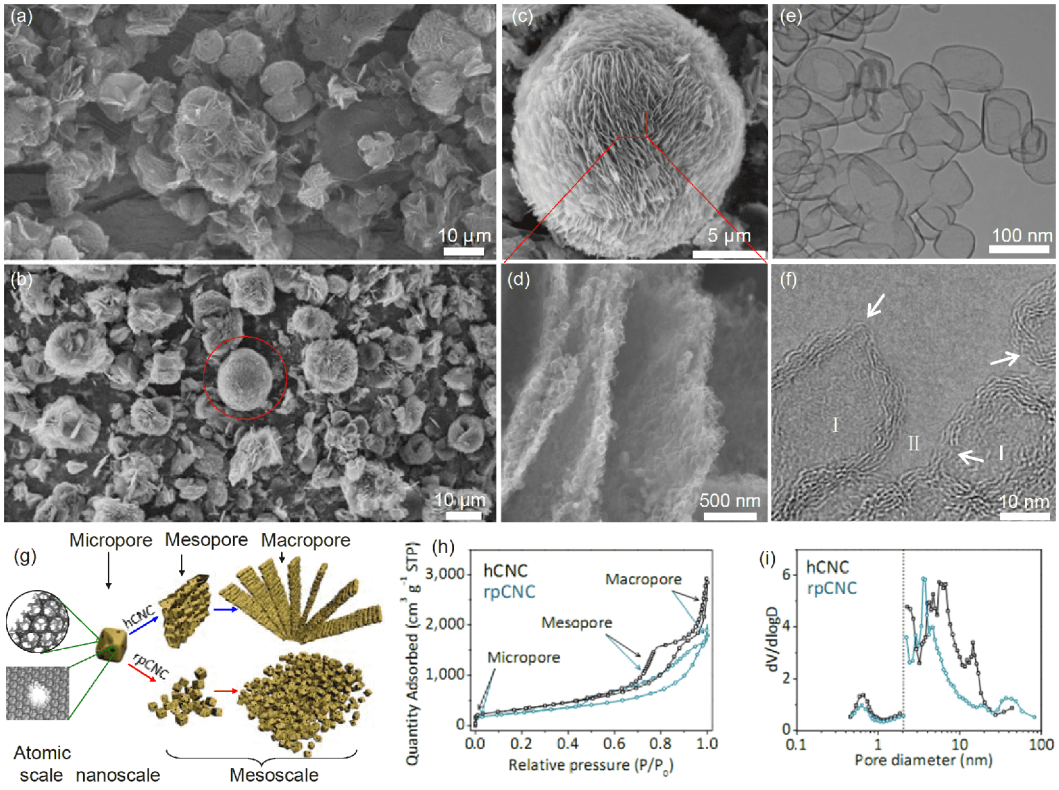

Figure 4 Comparison of mesostructured hierarchical carbon nanocages (hCNC) and randomly packed carbon nanocages (rpCNC). (a) Scanning electron microscope (SEM) image of mesostructured basic magnesium carbonate. (b) SEM image of the mesostructured carbon nanocages. (c–f) Typical SEM and transmission electron microscope (TEM) images. Arrows in (f) indicate the broken fringes. Regions I and II represent the spaces inside the nanocages and interspace between the nanocages, respectively. (g) Schematic structural characters of the hCNC and rpCNC at multiscales. (h, i) N_2 adsorption/desorption isotherms and the corresponding pore size distributions of hCNC and rpCNC [13] (color online).

chemical vapor deposition with appropriate carbon precursors. In this process, the basic magnesium carbonate decomposes into *in-situ* generated MgO templates, and its morphology is passed down to the carbon products (Figure 4 (a, b)). After MgO templates were removed by acid etching, the hierarchical carbon nanocages (hCNCs) were obtained (Figure 4(b–f)). Such a unique morphology endows the hCNCs with high SSA (up to 2,700 $m^2 g^{-1}$), large pore volume (2–5 $cm^3 g^{-1}$) and coexisting micro-meso-macropores (Figure 4(h, i)) [10,13,20].

The size and shell thickness of the carbon-based nanocages can be conveniently regulated by controlling the growth temperature and feedstock. In general, the higher growth temperature leads to the larger sizes and higher graphitization of the nanocages. The SSA of the carbon nanocages depends on the dosage of carbon precursors, which can be regulated in the range of 300–2,700 $m^2 g^{-1}$. The complete removal of MgO templates reflects the unsealed feature of the carbon-based nanocages. Moreover, the heteroatom-doped carbon nanocages can be easily synthesized by a similar procedure with different carbon precursors (such as benzene, pyridine, and thiophene) [10,33,41–43]. With pyridine as the carbon precursor, hierarchical N-doped carbon nanocages (hNCNCs) were obtained with the tunable nitrogen contents in the range of 0 at%–13 at% depending on the growth temperature [41]. With thiophene precursors, hierarchical sulfur-doped carbon nanocages (hSCNCs) with the sulfur content of 0 at%–4 at% were obtained [42]. The hierarchical codoped carbon nanocages were also facilely prepared by using mixed precursors with different heteroatoms [43]. It is worth noting that the *in-situ* MgO template synthesis can be scaled up for mass production.

Besides the common features of carbon nanocages including the hollow interior cavities with subnanometer microchannels across the shells, the high SSA with abundant topological defects on the outer surface, and the tunable electronic structure by easy doping of heteroatoms, the mesostructured carbon-based nanocages own the hierarchical architecture and interconnected micro-, meso- and macropores favoring mass/charge transfer [10,13]. Such unique structures and morphologies make them very different from the 1D carbon nanotubes (CNTs) with relatively inert surface and limited surface area, the 2D graphene suffering from π-π restacking and doping difficulty. The mesostructured carbon nanocages are also very different from the individual or randomly packed carbon nanocages without well-developed pore structures (Figure 4(g–i)) [10,13].

The assembly manner of hollow carbon-based nanocages

into 3D mesostructures can be modulated by using different templates or procedures, as typically shown in Figure 5 [44–46]. The 3D hierarchical N-doped carbon nanocages were synthesized by impregnating the poly(methylmethacrylate) (PMMA) nanospheres into the dopamine solution, followed by the carbonization at 800 °C under N_2 atmosphere. The mesostructured morphology was inherited from the ordered array of the interconnected PMMA nanospheres (Figure 5 (a)). When the PMMA@polydopamine composite was further impregnated by cobalt acetate solution, 3D interconnected Co-N-doped carbon nanocages were obtained [44]. By using bimodal polymer-silica colloidal crystals, the 3D ordered macroporous carbons with the walls composed of hollow mesosized nanocages were prepared. That is, small silica colloids were filled into the macropores among the orderly-packed large colloids of poly[styrene-(*co*-2-hydroxyethyl methacrylate)], and the composite was heated at 100 °C to interconnect the polymer particles, followed by the carbonization and carbon coating of the silica colloids. After removing the silica, the interconnected small nanocages with 3D ordered macropores were prepared (Figure 5(b)) [45]. A pomegranate-like hierarchical porous carbon clusters were fabricated by a spray drying of SiO_2@SiO_2/RF (RF= resorcinol formaldehyde) nanospheres, followed by carbonization and silica-template etching, which were composed of numerous hollow nanocages and a thin, microporous sheath (Figure 5(c)). Such a mesostructure integrates microporous, mesoporous and hollow nanostructures into a micrometer-sized particle, which could embody the merits and mitigate the shortcomings of every individual component [46].

The hierarchical mesostructures of carbon-based nanocages and other nanocarbons such as CNTs and graphene

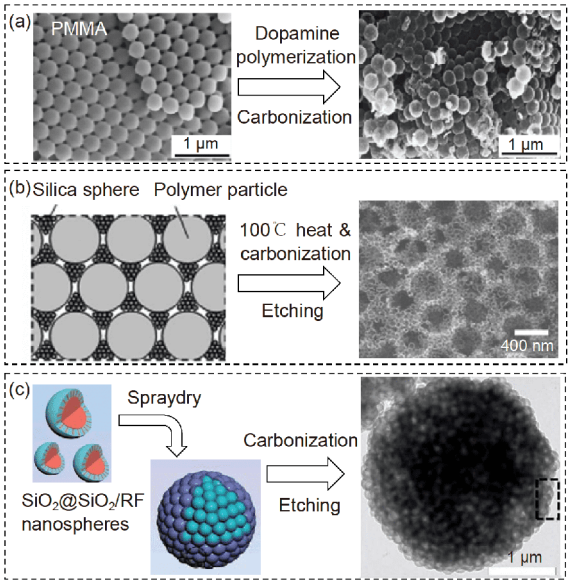

Figure 5 Other synthetic routes to mesostructured carbon-based nanocages. (a) With PMMA templates [44]; (b) with bimodal polymer-silica colloids templates [45]; (c) by a spray drying method [46] (color online).

were also constructed for energy chemistry applications [47–51]. The carbon microtube-confined hollow nanocages were synthesized by filling silica colloids into the channels of anodic alumina oxide templates, followed by the evaporation coating of pyrrole, carbonization and template removal. The unique hollow "nanocages-in-microtube" architecture provides a large SSA, high heteroatom content, and hierarchical porous structures, with great promise for ECS [47]. The hierarchical carbon mesostructures of nanocages hanging on CNTs were grown by depositing Au nanoparticles on CNTs and subsequent electric Joule heating for carbon coating and Au evaporation [48]. Graphene can act as substrates or spacers to construct the composite with carbon-based nanocages [49–51]. The mesostructured composite of N-doped carbon nanocages and reduced graphene oxide (rGO) was prepared by self-assembling SiO_2@polydopamine-GO hierarchical structure, followed by the heat treatment and HF-NH_4F etching. The hollow nanocages act as spacers to separate rGO nanosheets, which prevents the aggregation of graphene, ensuring the fast mass/charge transport and better electrochemical performances [49]. The composite of graphene layers embedded with graphitic carbon nanocages (G-GCNs) was obtained by growing Fe_xO_y nanoparticles on functionalized graphene followed by hydrothermal carbon coating and high temperature carbonization. Such a composite owns a high SSA of 1,210 $m^2\ g^{-1}$, total pore volume of 1.01 $cm^3\ g^{-1}$, high conductivity and structure stability, favorable for energy storage [50]. The monoliths of carbon nanocages and rGO were conveniently formed by dispersing preformed nanocages into the GO solution, followed by self-assembly of hydrogels in the presence of vitamin C. The carbon nanocages were embedded in the matrix of rGO, which facilitates the charge transfer kinetics [51]. The preceding examples demonstrate the tunable morphologies of mesostructured carbon-based nanocages, which are quite different from the individual nanocarbons.

As demonstrated in the preceding part, the mesostructured carbon-based nanocages possess the unique features with the big accessible interior cavities for the confinement, hierarchical porous structure and scaffold for smooth mass/charge transfer, as well as the high SSA and tunable electronic structures, much different from the other nanocarbons, or the individual/randomly-packed nanocages. By utilizing these structural characteristics, the mesostructured carbon-based nanocages and their composites by supporting or encapsulating foreign materials much enrich the contents in energy chemistry as schemed in Figure 6 and summarized in the following part.

3 Applications in energy storage

The unique hierarchical porous structure and netlike frame-

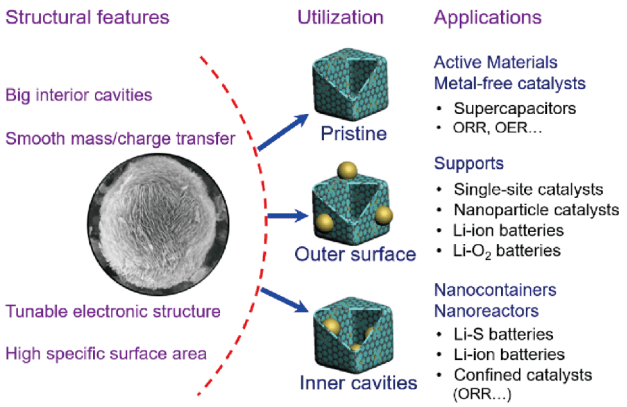

Figure 6 Schematic strategies for wide applications of mesostructured carbon-based nanocages (color online).

work endow the mesostructured carbon-based nanocages and their composites with fast mass/charge transfer kinetics, showing great advantages in high-rate energy storage. Moreover, the unique big interior cavities of the nanocages are very suitable for encapsulating various foreign active materials, and their outer surface with abundant topological defects (holes, edges, pentagons, *etc.*) and/or heteroatom dopants is convenient to support different foreign species with high dispersion. Usually, the pristine mesostructured carbon-based nanocages and their composites are efficient electrodes for supercapacitors and rechargeable batteries with high utilization efficiency, excellent rate capability and superior cycling stability, as demonstrated below.

3.1 Supercapacitors

Carbon-based materials store charges *via* electrostatic adsorption on the surface, and thus the regulation on their SSA, surface/electronic structures and charge-transfer alleyway is crucial to improve the capacitive performance. CNTs and graphene have been intensively studied as electrodes for supercapacitors; however, the low SSA of CNTs and the π-π restacking of graphene limit their capacitances [52,53]. Mesostructured carbon-based nanocages can remain the large SSA and well-balanced pore structures by avoiding π-π restacking, which provide sufficient spaces for charge storage, free highway for mass transport and interconnected framework for electron transfer, presenting great promise for supercapacitors. For the hCNCs grown by *in-situ* MgO template method, the SSA was conveniently tuned by changing the growth temperature and the dosage of precursors. The hCNCs with the SSA of 1,854 $m^2 g^{-1}$ exhibited a high capacitance of 260 F g^{-1}@0.1 A g^{-1} and a quite good stability with 90% retention after 10,000 cycles in 1 M H_2SO_4 solution [32]. The hCNCs synthesized by using silica colloids as hard templates and furfuryl alcohol as carbon source owned easy-accessible large SSA and high conductivity, delivering a high specific capacitance of 240 F g^{-1}@1 A g^{-1}. When they were activated by KOH, a higher capacitance of 304 F g^{-1} was achieved at 1 A g^{-1} [54]. The 3D hCNC networks by nano-coating carbon precursors on flower-like basic magnesium carbonates, carbonization and KOH treatment delivered the specific capacitance of 288 F g^{-1}@1 A g^{-1} and still maintained 256 F g^{-1}@10 A g^{-1} [55]. The "nanocages-in-microtubes" mesostructure exhibited a specific capacitance of 235 F g^{-1}@0.2 A g^{-1} and 156 F g^{-1}@20 A g^{-1} in 6 M KOH solution, much higher than that of hollow nanocages, microtubes, or even the mixture of hollow nanocages and microtubes, showing the promotion effect of the mesostructures [47].

Though the capacitance of hCNCs is much higher than that of graphene, the area-normalized capacitance of hCNCs is still far below the theoretical limit of carbon (21 μF cm^{-2}) owing to the hydrophobic nature of pristine carbon [56]. Heteroatom-doping is an efficient strategy to improve the surface wettability and increase the ion-accessible surface area thereof. By N-doping, the specific capacitance was increased from 13.4 μF cm^{-2}@1 A g^{-1} for the hCNC to 17.4 μF cm^{-2}@1 A g^{-1} for the hNCNCs in 6 M KOH solution (Figure 7(a)). The N-doping turned the hydrophobic hCNCs into highly hydrophilic hNCNCs (Figure 7(a-i)), which much reduced the charge transfer resistance and equivalent series resistance of the device (Figure 7(a-ii)). Thus, the ion-accessible surface was effectively increased, and the area-normalized capacitance was improved thereof [34]. This result suggests an efficient and general strategy to improve the supercapacitive performance by suitable heteroatom doping. The power density, another important factor of carbon-based supercapacitors, can be improved by increasing the electric conductivity of carbon electrodes. We replaced the *in situ*-generated MgO template by the *in situ*-generated Cu template, and the obtained porous 3D few-layer graphene-like carbon possesses much better conductivity with the directly connected meso- and macropores owing to the low melting point of Cu. The symmetric supercapacitor presents the ultrahigh maximum power densities of 1,066.2 and 740.8 kW kg^{-1} in aqueous and ionic liquid electrolytes, respectively, showing top-level power density without scarifying the high energy density [57].

The highly porous carbon-based nanomaterials are beset with low density, which heavily limits the volumetric energy density of supercapacitors. As known, the volumetric energy density is more important for many practical applications, especially when the supercapacitors are used in a limited space to drive compact electronic devices. Actually, the micropores and smaller mesopores provide the room for charge accommodation, while the larger mesopores and macropores have little contribution to the capacitance but lead to the low density and inferior volumetric energy density thereof. Thus, reducing the surplus spaces within the macro- and mesopores is promising to improve the volu-

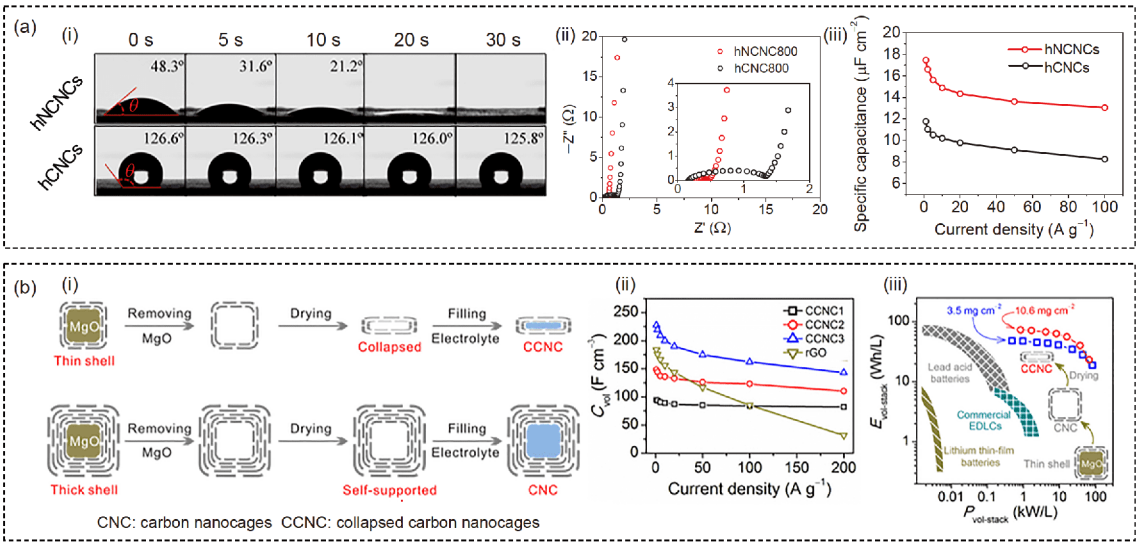

Figure 7 Supercapacitive performances of mesostructured carbon-based nanocages. (a) Enhancing the capacitive performances by N-doping [34]. (i) Dynamic water contact angle measurement; (ii) Nyquist plots; (iii) area-normalized capacitances at different current densities. (b) Enhancing the volumetric performances by capillary compression [35]. (i) Preparation procedures; (ii) volumetric capacitances at different current densities in 6 M KOH; (iii) Ragone plots of the electrode stack in $EMIMBF_4$ (color online).

metric energy density. Many methods such as liquid-mediated dense integration and H_2O_2 etching-compression have been developed to increase the density of graphene, which, however, usually delivered the volumetric energy density below 60 W h L^{-1} [58,59]. We compressed the carbon nanocages with ultrathin shells *via* capillarity by simple drying process. The carbon nanocages with collapsed interior cavities (CCNC) owns a high density up to 1.32 g cm^{-3}, while the partially compressed porous structure still remains high SSA and fast charge transfer kinetics, which increases the volumetric capacitances to 228 F cm^{-3} in 6 M KOH and 233 F cm^{-3} in $EMIMBF_4$ ionic liquid at 1 A g^{-1}. The optimized sample achieved a record-high stack volumetric energy density of 73 W h L^{-1} in ionic liquid with a maximal stack power density of 67 kW L^{-1} and high stability, locating at the state-of-the-art level for compact carbon-based materials (Figure 7(b)) [35]. The volumetric performance could be further improved by compressing heteroatom-doped carbon nanocages to achieve the balance between the high density and the ion-accessible surface.

Considering the high theoretical capacitances of pseudocapacitive materials such as transition metal compounds, their hybridization with mesostructured carbon-based nanocages is an efficient route to enhance the energy density of the supercapacitors. The hybridization can downsize the active component and enhance the charge transfer kinetics, thus leading to high energy storage performance. Tiny $Co(OH)_2$ nanocrystals were conveniently immobilized on the surface of hNCNC with high dispersion and uniformity. The optimized $Co(OH)_2$/hNCNCs hybrid achieved a high specific capacity of 1,170 F g^{-1}@2 A g^{-1}, in which the capacitance of $Co(OH)_2$ (2,214 F g^{-1}) is close to its theoretical maximum (2,595 F g^{-1}) [60]. Similar enhancement can be found in the 3D network of carbon nanocages/V_2O_5 nanosheets and the ultrathin MoS_2 nanosheets decorated hCNCs [61,62]. The progress demonstrates the great potential of mesostructured carbon-based nanocages in supercapasitors either as the electrode material or as the platform for hybridization.

3.2 Lithium-ion batteries

A challenging issue for LIBs is to achieve the large reversible capacity, high rate capability and good cycling stability simultaneously. The hCNCs anode exhibited a high specific capacity and high-rate capability, with a high reversible capacity of 970 mA h g^{-1}@0.1A g^{-1} after 10 cycles, and a remained capacity of 229 mA h g^{-1} after 10,000 cycles at a high rate of 25 A g^{-1}. The superior performance originates from the unique morphology of hCNCs with the large SSA, multiscale pore structure and high conductivity, which synergistically favor the electrolyte penetration, solid-state ion diffusion, electron conduction and structural stability [63]. The 3D carbon-based nanocages can act as the supports to hybrid with suitable metal compounds, which usually show excellent lithium storage performances. 3D ordered CNCs derived from PMMA templates and RF precursors were used to construct a MnO_2/CNCs composite with hierarchical hollow structures. The reversible capacity of 420 mA h g^{-1} was achieved at 1 A g^{-1} based on the whole mass of the composite, higher than the theoretical value of 372 mA h g^{-1} for commercial graphite. The superior electrochemical performance can be attributed to the improved ion/electron transportation due to the conductive CNCs and

porous structures for retarding the volume changes of MnO_2 during Li^+ insertion/extraction [64]. The ultrathin SnS nanosheets decorated CNCs can crosslink with rGO to form 3D interconnected networks, showing high charge capacity, distinguished cycling stability (1,027 mA h g^{-1}@0.2 A g^{-1} after 100 cycle), and good rate capability for LIBs [65]. The hierarchical nanocomposite of ultrathin WS_2 nanosheets on the surface of N-doped CNCs exhibited a high specific capacity of 801.4 mA h g^{-1}@0.1 A g^{-1}, excellent rate capability (545.6 mA h g^{-1}@2 A g^{-1}) and great cycling stability with a capacity retention of 95.8% at 0.5 A g^{-1} after 150 cycles [66]. Vertically grown few-layer MoS_2 nanosheets on hCNCs presented pseudocapacitive-dominated lithium storage, showing a high reversible capacity (1,670 mA h g^{-1}@0.1 A g^{-1}), high-rate capability and superb long-term recyclability (236 mA h g^{-1}@25 A g^{-1} after 3,000 cycles), among the best for the reported MoS_2-based materials [67]. The progress demonstrates the great potential of the hierarchical carbon-based nanocages and their composites in LIBs owing to the synergism of facilitating fast electron/ion transfer, accommodating mechanical stress from cycling, restraining agglomeration and enabling full utilization of the active materials. By encapsulating the active materials inside CNCs, recently we developed a simple and general strategy to construct the yolk-shelled metal oxides inside hCNC to further facilitate the mass/charge transfer, as shown in Figure 8. The obtained MO_x@hCNC provides sufficient interior voids to buffer the large volume variation, forms the stable solid electrolyte interface (SEI) film (Figure 8(d)), and greatly reduces the loss of active components during lithiation/delithiation. As an example, the SnO_2@hCNC exhibits a superior rate capability to the most SnO_2-based anode materials reported to date, including the control sample of SnO_2/hCNC with SnO_2 outside the nanocages (Figure 8(b, c)) [68]. Such an approach to the yolk-shelled MO_x@hCNC is significant for exploring the high-performance electrode materials for LIBs or even beyond [69].

3.3 Lithium-sulfur batteries

The lithium-sulfur (Li-S) batteries are one of the most attractive energy storage devices for the high theoretical capacity and low cost. The main hindrances for practical applications include the insulation of S/Li_2S decreasing sulfur utilization, the shuttle effect losing active components, the polarization effect increasing overpotential, and the big volumetric change pulverizing electrodes during cycling [70]. Carbon-based nanocages are demonstrated as effective hosts for sulfur to address the above issues as shown in Figure 9.

Physically confining sulfur within porous carbon-based materials can decrease the loss of lithium polysulfides (LiPSs), increase the conductivity, and meanwhile accommodate the volumetric expansion, which becomes an efficient way to improve the Li-S battery performance [71]. With the semi-hermetic interior cavities of the large pore volume, carbon nanocages are excellent nanocontainer to encapsulate high-loading sulfur for Li-S batteries [72]. By taking the mesostructured carbon-based nanocages with the fast charge/mass transfer kinetics as discussed above, the S@hCNCs cathode presents a high-rate capability. Specifically, the S@hCNCs with a high sulfur content of 79.8 wt% achieved a large discharge capacity, high-rate capability (580 mA h g^{-1}@3 A g^{-1}), and long cyclability

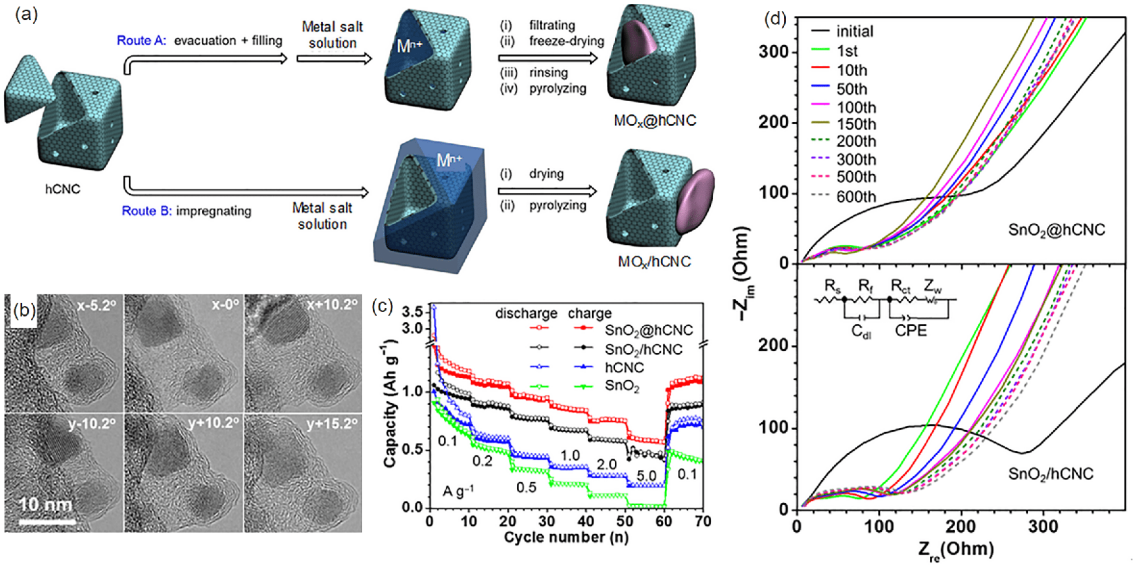

Figure 8 Encapsulating and supporting metal oxides for LIBs [68]. (a) Schematic preparation route. (b) Tilting TEM images of SnO_2@hCNC. (c) Rate capabilities of different SnO_2-based samples in LIBs. (d) Nyquist plots of SnO_2@hCNC and SnO_2/hCNC before cycling and after different cycles (color online).

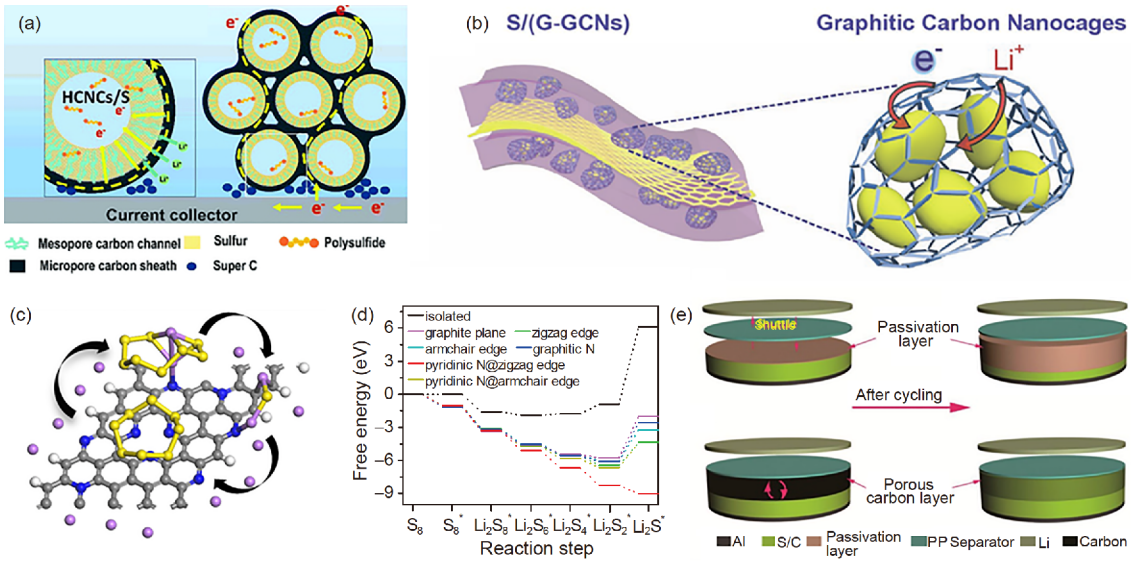

Figure 9 Strategies for improving the Li-S battery performance with carbon-based nanocages. (a) Illustration of facilitated charge transfer and conversion reactions [46]. (b) S@G-GCNs with suppressed shuttle effect and volume swelling/shrinkage, and enhanced charge transfer kinetics [50]. (c, d) Combined electrocatalysis and adsorption effects of N-doped carbons and the calculated free energies in the conversion reactions [36]. (e) Schematic illustration of the contribution of high conductive carbon nanocages modified separators [75]. Upper: a routine polypropylene (PP) separator; bottom: a carbon nanocage-modified separator (color online).

(558 mA h g^{-1}@1 A g^{-1} over 300 cycles). Such a performance is much superior to the cathode of sulfur filled in randomly packed carbon nanocages, demonstrating the great contribution of the mesostructures of hCNCs [13]. The pomegranate-like carbon clusters composed of numerous hollow nanocages and a thin, microporous sheath integrate the large void space, radial mesoporous pathways and conductive networks. When high loading sulfur was encapsulated, the obtained cathode demonstrated high rate performances and low fading rates, with a high discharge capacity of 592 mA h g^{-1}@8 A g^{-1}, and a retained capacity of 695 mA h g^{-1}@0.32 A g^{-1} after 500 cycles. The superior performance results from the alleviation of the dissolution and shuttling of LiPSs (Figure 9(a)) [46]. Hierarchical mesostructures composed of aligned porous graphene and interconnected nanocages can facilitate the infiltration of electrolytes and the transport of ions as well as improve the charge storage capability. Hence, this hierarchical composite of graphene-CNCs can load sulfur at a higher mass loading, and delivered high specific capacity of 1,640 mA h g^{-1}@0.1 C with high cycling stability [73]. The S@G-GCNs demonstrated a superior battery performance, including the high specific capacity (initial 1,375 mA h g^{-1}@0.1 C), favorable high-rate capability (765 mA h g^{-1}@5 C), and excellent long-term cycling stability (1,000 cycles) owing to the suppressed shuttle effect and volume swelling/shrinkage, and enhanced charge transfer kinetics (Figure 9(b)) [50].

To further suppress the shuttle effect of LiPSs, polar materials were filled inside or supported outside the nanocages to chemically adsorb the soluble LiPSs. The porous composite of N-doped hollow CNCs and 3D graphene frameworks (NHC-GFW) was used to encapsulate sulfur, which exhibited a considerably high capacity, an excellent rate performance, and a long-term cycling stability [74]. The NHC-GFW efficiently suppressed the shuttle effect *via* physical confinement and chemical adsorption, and thus improved the electrochemical performance of Li-S batteries. We employed the hNCNCs as the sulfur host and the interlayer on separators, and the Li-S@hNCNCs battery presented the record-high power density of 9.2 kW kg^{-1} at a high energy density of 249 W h kg^{-1} and an excellent high-rate cycling stability with a high capacity of 438 mA h g^{-1} even after 1,000 cycles at an ultrahigh current density of 10 A g^{-1}. The combined experimental and theoretical studies revealed that the N-doped sp^2-carbon has highly-efficient catalytic functions to LiPSs conversion, beyond the previously reported chemical adsorption functions (Figure 9(c, d)) [36]. The synergism of physical confinement, chemical adsorption, electrocatalytic promotion and facilitated mass/charge transfer contributes to the durable high-power cathode for Li-S batteries. This finding demonstrates the metal-free catalytic function of the heteroatom-doped carbons to LiPSs conversion for the first time, which enriches the applicability of carbon-based metal-free catalysts. To further illuminate the electrocatalytic function of heteroatom-doped sp^2-carbon to the LiPSs conversion, the hSCNCs were adopted to encapsulate sulfur (S@hSCNCs). The as-obtained sulfur cathode exhibited a high capacity of 579 mA h g^{-1}@2 A g^{-1} after 400 cycles, obviously better than the counterpart using undoped hCNCs [42]. As known, the interaction between the soluble LiPSs and the S-doped

carbon is weaker than that between the LiPSs and the pristine carbon; hence the better performance of S@hSCNCs than S@hCNCs was ascribed to the electrocatalytic mechanism of S-doped carbon. These results suggested the general electrocatalytic function of heteroatoms-doped carbons to the LiPSs conversion, providing a new angle to explore advanced electrode materials for Li-S batteries especially by combining the advantages of mesostructured carbon-based nanocages with physical confinement, electrocatalysis and facilitated transport kinetics.

The areal capacity of Li-S batteries is an important factor for practical applications. Increasing the sulfur loading can improve the areal capacity, but the mass/charge transfer was also impeded with increasing the electrode thickness, usually leading to inferior battery performances. We constructed free-standing monolithic sulfur cathodes of rGO wrapped S@hCNCs (S@hCNCs@rGO), which exhibited top-ranking areal capacity of 3.7 mA h cm^{-2} with the high areal sulfur loading of 3.8 mg cm^{-2}, owing to the synergism of the physical confinement of hCNCs, the chemical adsorption of oxygen functional groups on rGO, the accelerated charge transfer kinetics arising from the hierarchical porous structure and high electrical conductivity [51]. The hierarchical electrode of S@hSCNCs also presented a high areal capacity of 4.7 mA h cm^{-2} with a high sulfur loading of 4.5 mg cm^{-2} owing to the unique porous mesostructure of hSCNCs [42]. By using the highly conductive 3D porous CNCs as separators and sulfur hosts, the areal sulfur loading and areal capacity can achieve 7.34 mg cm^{-2} and 2.5 mA h cm^{-2}, respectively [75]. The enhancement can be ascribed to the high conductivity of porous CNCs by promoting the solid to liquid phase transformation reactions and buffering the shuttling effect (Figure 9(e)). These results suggest the great potential of the hierarchical carbon-based nanocages in the practical Li-S batteries.

3.4 Other rechargeable batteries

The mesostructured carbon-based nanocages can also hybrid with other active components for various batteries. For instance, the porous hCNCs with interconnected hollow bubbles of ~20 nm and shell thickness of ~5 nm were filled with Se species by melt-infiltration methods for Li-Se batteries. The composite delivered an initial specific capacity up to 588.2 mA h g^{-1}@0.5 C, exhibiting an outstanding cycling stability over 500 cycles with a decay rate even down to 0.08% per cycle. This electrode material retained the capacity of 200 mA h g^{-1} even after 1,000 cycles at 1 C, much superior to the Se cathode prepared using carbon black and bulk Se. The excellent performance was ascribed to the distinct hollow structure of the carbon spheres and a large amount of Se wrapped within the small carbon bubbles [76].

Reversible lithium-oxygen (Li-O_2) batteries are the most ideal alternative power sources for their high theoretical energy density [77]. The hCNCs with porous structure and high conductivity are promising cathode materials, which is beneficial to increase the capacity of Li-O_2 battery by accommodating more discharge products of Li_2O_2. The 3D porous frameworks of N-doped graphene and interconnected nanocages delivered a high specific capacity, excellent rate capacity and cycling stability owing to the well-balanced pore structure and the full exposure of electrochemically active sites [78]. The performance of Li-O_2 batteries could be further enhanced by supporting the catalysts on hCNCs to enhance oxygen reactions, which will be introduced in the later part owing to the involvement of electrocatalysis [79].

4 Applications in energy conversion

Energy conversion is a sustainable and effective strategy to utilize renewable energies, and exploring the advanced catalysts is always a crucial and hot issue. The commercial or benchmark catalysts for many energy-related reactions are platinum-group metals (PGM), which are often beset with the high price, easy deactivation and poor durability. The main objectives of this field focus on the development of lower-PGM-loading catalysts, non-precious-metal (NPM) catalysts or even metal-free catalysts. In virtue of the advantages of mesostructured carbon-based nanocages with large interior cavities and hierarchical conductive frameworks, high exposed surface and easy doping, various PGM or NPM-based catalysts from single-sites to nanoparticles can be conveniently supported outside or encapsulated inside the nanocages as shown in Figure 10 [37,40,80,81], which benefits the efficient utilization of active species, the fast mass/charge transport and the long durability. The mesostructured carbon-based nanocages are also the efficient metal-free electrocatalysts for suitable energy conversion reactions owing to the large SSA, defective surface and tunable electronic structures [33,38]. These merits lead to the wide applications in energy conversion.

4.1 Oxygen reduction reaction catalysts

Sluggish oxygen reduction reaction (ORR) is the bottleneck for fuel cells and metal-oxygen batteries [82], which was promoted by Pt catalysts in commercial applications. Usually, the Pt catalysts suffer from the low Pt utilization, gradual deactivation, detachment or aggregation as well as the alcohol crossover effect when working in direct alcohol fuel cells [83]. The cheap and durable ORR catalysts are highly expected [84]. The mesostructures of hollow core-mesoporous shell carbon can achieve the uniform dispersion of Pt nanoparticles with high loading (60 wt%) owing to their large SSA and mesoporous volume, and the well-

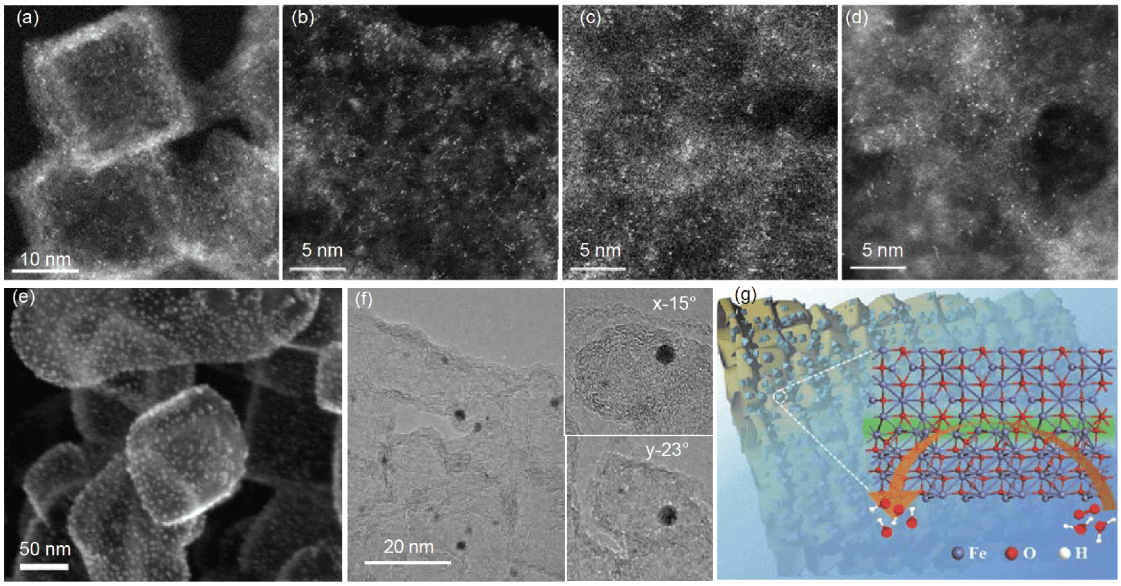

Figure 10 PGM or NPM-based catalysts constructed with the hierarchical carbon-based nanocages. (a–d) Single-site catalysts of Pt (a), Pd (b), Au (c) and Ir (d) [40]. (e) Pt nanoparticles on hNCNCs [80]. (f) Pt nanoparticles filled inside hNCNCs [37]. (g) α-Fe_2O_3/Fe_3O_4/hNCNCs electrocatalysts with abundant nano-heterointerfaces [81] (color online).

developed 3D interconnected porous network facilitates the fast mass/charge transport. Hence, the as-prepared Pt (60 wt%) catalyst demonstrated the markedly enhanced catalytic activity for ORR compared with that on Vulcan XC-72 supports. The PEMFC polarization performance was greatly improved even at a low catalyst loading of 0.2 mg_{Pt} cm^{-2} [85]. As known, the incorporation of heteroatom dopants could tune the distribution and electronic structures of active phases, in which the nitrogen-doping is particularly intriguing [20]. Taking advantage of the N-incorporation and high SSA, the Pt nanoparticles were highly dispersed on the hNCNCs *via* a convenient microwave-assisted ethylene glycol reduction, which have the uniform size of 2.6±0.4 nm with the mass loading of 23.6 wt% (Figure 10(e)). The Pt/hNCNCs displayed similar ORR activity with onset potential of ca. 937 mV (*vs*. RHE) but superior durability to the commercial Pt/C [37]. It is widely accepted that the N-participation could efficiently enhance the binding energies of Pt on the carbon supports and modify the electronic states, which enables the easy construction and durable use of nanocomposite catalysts [20].

Encapsulating Pt nanoparticles inside the carbon-based nanocages is efficacious to alleviate their dissolution and detachment. By a vacuum-filling method, we encapsulated the Pt nanoparticles inside the hNCNCs (Pt@hNCNCs) with the average size of 1.3±0.3 nm and the mass loading of 19.3 wt% (Figure 10(f)). The Pt@hNCNCs exhibited high ORR durability in acidic media, although its ORR onset potential (906 mV *vs*. RHE) was slightly lower than that of Pt/hNCNCs. More interestingly, the Pt@hNCNCs presented excellent tolerance to alcohol crossover. Such a different performance for the Pt nanoparticles inside *versus* outside the nanocages is correlated with the molecule-sieving effect of the microchannels across the shell. Specifically, the microchannels with the size of ~0.6 nm admit the small-sized oxygen and ions into the nanocages with a certain hindrance, while block the large-sized alcohols and Pt species, leading to the high immunity to alcohol crossover and high durability [37]. Similar performance was also observed in the case of Au nanoparticles encapsulated inside the hNCNCs [86]. The yolk-shell structure with size-sieving effect, as well as the hierarchical porous structure with facilitated mass/charge transfer kinetics endows such encapsulated catalysts with outstanding catalytic activity, selectivity and stability. It is mentioning that the vacuum-filling method is generally applicable to various materials, superior to the encapsulation by *in-situ* formation of carbon coating out of the target materials [10,68], which provides more opportunity to explore advanced catalysts.

Taking advantage of the mesostructured porous structure and the heteroatom participation of carbon-based nanocages, various NPM catalysts for ORR were constructed to further decrease the cost of ORR catalysts and immunize the alcohol crossover effect. The high dispersion of active phases can increase the density of active sites and the catalyst utilization efficiency. In addition, the charge transfer between transition metals and N-doped carbons leads to the modification of electron structures of supported nanoparticles, usually resulting in the better electrocatalytic performance [81,87,88]. For example, the alloyed Co-Mo nitride nanoparticles supported on hNCNCs showed superior ORR performances to the counterparts supported on carbon nanocages in acidic

media, and moreover the Co-Mo alloying endowed the active nitrides with the high activity (onset potential: 808 mV *vs*. RHE) of cobalt nitride and the high stability of molybdenum nitride, outperforming most NPM based catalysts [87]. The α-Fe_2O_3/Fe_3O_4/hNCNCs electrocatalyst with abundant nano-heterointerfaces (Figure 10(g)) exhibited excellent ORR performances surpassing the commercial Pt/C in alkaline media, with a high onset potential (1.03 V *vs*. RHE), robust durability and methanol tolerance [81]. The metal/nitrogen/carbon materials are eye-catching NPM electrocatalysts for ORR in either acidic or alkaline media, and the high exposure of the M-N_x active sites is crucial to realize the full potential of these catalysts [82]. To this end, manganese oxide nanoparticles were highly dispersed on the hNCNCs owing to the N-participation, followed by a manganese oxide-induced polymerization strategy to obtain the polyaniline (PANI) film uniformly coated on the hNCNCs, *i.e.*, PANI/hNCNCs. Then, the $FeCl_3$ impregnation and the high-temperature treatment of $FeCl_3$/PANI/hNCNCs composites led to the Fe/N/C catalyst with highly exposed Fe-N_x active sites. The constructed Fe/N/C catalysts presented a high onset potential of 920 mV (*vs*. RHE), comparable to the Pt/C benchmark catalyst in activity but with much better stability. By contrast, the Fe/N/C catalyst constructed by the undoped hCNCs without the N-participation is inferior in ORR performance owing to the partial embedment of active sites [87].

In the past decade, carbon-based metal-free catalysts have attracted extensive interests since the first discovery of the excellent ORR activity of nitrogen-doped carbon nanotube arrays in alkaline media [89–91]. Carbon-based nanocages are highly potential ORR catalysts owing to their large SSA, tunable electronic/surface structure and convenience for metal-free synthesis. In virtue of the metal-free synthesis, we confirmed that the high ORR activity of hNCNCs resulted from the N-doped carbon species, rather than the metal-related species [33]. With the assistance of theoretical simulation, we supposed a general strategy to turn ORR-inert sp^2 carbon into ORR-active by activating the carbon π electrons, which can be achieved by doping with either electron-rich (*e.g.*, N) or electron-deficient (*e.g.*, B) dopants [92]. This motivated the subsequent development of ORR catalysts by doping/codoping carbon-based nanocages with different heteroatoms (*e.g.*, N, B, S, P) [93,94]. This strategy of activating carbon π electrons also suggested that the intrinsic defects in sp^2 carbon could promote ORR activity, which was confirmed by the superior ORR performance of the hCNCs with abundant pentagons, edges, holes and corners [38]. Theoretical calculations revealed the pentagon and zigzag edge defects contributed to the high ORR activity [38]. A very recent result also demonstrated the high ORR activity of defects in acidic media [95]. The progress extends the metal-free catalysts from heteroatom-doped sp^2 carbons to dopants-free ones, and meanwhile suggests a promising strategy to explore advanced carbon-based metal-free electrocatalysts by combining suitable intrinsic defects with dopants.

4.2 Alcohol oxidation catalysts

Direct alcohol fuel cells are attractive power sources for movable electric devices owing to their high energy conversion efficiency and easy storage/transportation of fuels. By a microwave-assisted ethylene glycol reduction method, the Pt/hNCNCs catalysts with mass loadings of 20 wt%–60 wt% were conveniently prepared owing to the anchoring function of N dopants (Figure 10(e)), which exhibited excellent electrocatalytic activity and stability for methanol oxidation reaction (MOR), obviously better than the control catalysts supported on hCNCs and Vulcan XC-72. The Pt/hNCNCs with a heavy loading of 60 wt% was still stable without serious agglomeration, giving a high peak-current density per unit mass of catalyst of 95.6 mA mg^{-1} for achieving a high power density [80]. The hNCNCs derived from polyaniline and silica spheres was used to anchor Pt nanoparticles. The nitrogen-doping contributed to the nucleation and growth kinetics of Pt nanoparticles, leading to the formation of small particles of ~2.1 nm with uniform dispersion. The Pt/hNCNCs presented superior electrochemical activity, high CO-tolerance and long stability towards MOR, better than the Pt nanoparticles loaded on N-doped nanocages without mesostructures and the commercial Pt/C catalysts. The difference of MOR performance indicated the positive promotion of the unique hierarchical porous structure [96].

In comparison with methanol, ethanol is particularly attractive in virtue of its high theoretical energy density (8 kW h kg^{-1}), low toxicity, and availability from biomass production. However, most Pt-based electrocatalysts for the ethanol oxidation reaction (EOR) in acidic media are still limited by low mass activity and high susceptibility to CO poisoning. We introduced oxophilic SnO_x species into the Pt/hNCNCs to optimize the particle size of Pt species and increase the anti-poisoning capability of Pt. The obtained ternary Pt/SnO_x/hNCNCs electrocatalyst shows the high EOR performance in acidic media with a mass activity of 1,187 mA mg_{Pt}^{-1} and high durability, in comparison with the most reported catalysts to date [39]. The SnO_x neighboring Pt sites could boost the water dissociation to form adsorbed OH species (OH_{ad}), and help the removal of adsorbed CO on Pt sites for regeneration, thus boosting the EOR performance.

These results demonstrated the great potential of mesostructured carbon-based nanocages in the exploration of high-efficient electrocatalysts to alcohol oxidation, and further studies can focus on the design of advanced catalysts with efficient multifunction integration by hybridization.

4.3 Hydrogen evolution reaction catalysts

Water electrolysis driven by renewable-derived electricity can provide clean hydrogen source for proton exchange membrane fuel cells. The high cost of the PGM electrocatalysts for hydrogen evolution reaction (HER) and oxygen evolution reaction (OER) hinders the practical application of water splitting. Decreasing the size of PGM nanoparticles is an efficient means to lower the catalyst cost. As the downsizing limit of supported catalysts, single-site catalysts (SSCs) are particularly attractive for the highest utilization of PGM atoms, and unique catalytic activity/selectivity. However, their convenient construction and durable utilization are highly challenging due to the high surface energy [97]. The Pt SSCs have been constructed on various carbon-based supports but the single-atom dispersion was usually achieved through complex procedures or harsh conditions, such as the high-temperature treatment, iced photochemical reduction, and atomic layer deposition [98]. Increasing the loading amount of Pt SSCs is crucial to applications but is a challenging topic [99]. Recently, we reported the simplest strategy to construct the single-site Pt atoms by an impregnation-adsorption process as shown in Figure 11. Thanks to the abundant micropores across the shells of carbon nanocages, $[PtCl_6]^{2-}$ ions were trapped into the ~0.6 nm micropores *via* van der Waals interactions, and the spontaneous dechlorination led to the formation of Pt single atoms on hCNCs with a slight aggregation (Figure 11(b, c)). Introducing N-dopants in the carbon nanocages can achieve the electrostatic interaction between the protonated pyrindinic N and the $[PtCl_6]^{2-}$ ion, further strengthening the metal-support interaction by the synergic micropore trapping and nitrogen anchoring. The isolated Pt single atoms were obtained with strong Pt–N interaction (Figure 11(a, c)) [40]. The Pt_1/hNCNCs catalysts with the Pt amount of 2.92 wt% exhibited a record-high electrocatalytic hydrogen evolution performance with low overpotential (η=15 mV@10 mA cm^{-2}), high mass activity (7.60 A g^{-1}@η=20 mV) and long stability ($\Delta\eta$=2.2 mV@50 mA cm^{-2} after 10,000 CV scans), much superior to the Pt-based catalysts to date including the Pt/C benchmark (Figure 11(d, e)). The Pt–N bonds are more stable than the Pt–C ones in the presence of adsorbed hydrogen atoms, leading to the superior stability of Pt_1/hNCNCs to that of Pt/hCNCs in hydrogen evolution. Thanks to the large SSA and the strong interaction of hierarchical carbon-based nanocages, the high loading (up to 5.68 at%) of Pt single-sites can be achieved. This strategy was also general for constructing the SSCs of other precious metals such

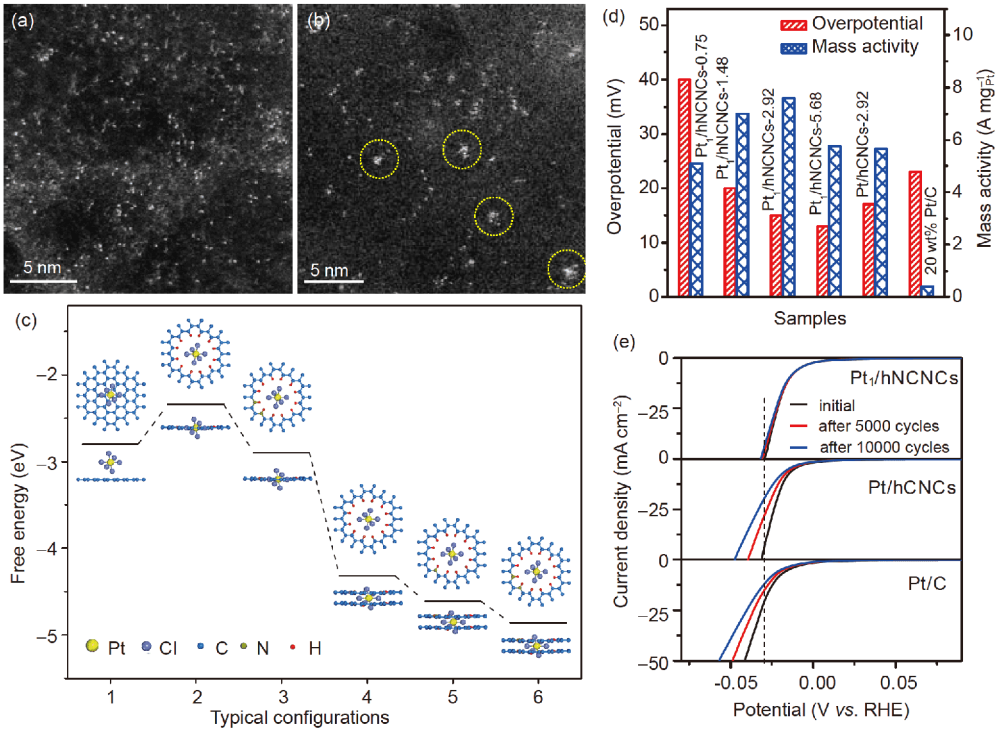

Figure 11 Construction of Pt SSCs with hierarchical carbon-based nanocages [40]. (a, b) High-angle annular dark-field scanning transmission electron microscopy (HAADF-STEM) images of Pt_1/hNCNCs (a) and Pt/hCNCs (b). (c) Six typical configurations of $[PtCl_6]^{2-}$ on different supports and corresponding calculated free energies. 1, graphene sheet. 2, graphitic mono-layer with a micropore of 0.6 nm. 3, graphitic mono-layer with the micropore decorated by two py-N atoms. 4, graphitic bi-layer with a micropore of 0.6 nm. 5, graphitic bi-layer with the micropore decorated by one py-N atom. 6, graphitic bi-layer with the micropore decorated by two py-N atoms. (d) Overpotentials at 10 mA cm^{-2} and mass activities at 20 mV (*vs.* RHE) of the series of catalysts in 0.5 M H_2SO_4 solution. The data for Pt/hCNCs and commercial Pt/C (20 wt% Pt) are presented for comparison. (e) Polarization curves of Pt_1/hNCNCs, Pt/hCNCs and commercial Pt/C before and after 5,000 and 10,000 CV scans (color online).

as Au, Ir and Pd, suggesting its great potential in exploring advanced SSCs by combining micropore trapping and dopant anchoring effects (Figure 10(a–d)) [40]. The subsequent studies could focus on the development of multi-atom and poly-metal SSCs by taking advantage of micropore trapping and dopant anchoring, and find their applications in advanced energy conversion reactions.

4.4 Oxygen evolution reaction catalysts

The carbon-based nanocages also showed the high OER activity as metal-free catalysts. The N-doped carbon nanocages prepared *via* an interfacial assembly demonstrated the improved OER activity and durability compared to the Pt/C electrocatalyst in alkaline media [100]. The B,N codoped carbon nanocages demonstrated to be a promising electrocatalyst for OER and HER, presenting a minimum overpotential of 0.39 V for OER and a lowest Gibbs free-energy of 0.013 eV for HER [101]. The 3D hierarchical Co-N-doped carbon nanocages synthesized by annealing PMMA-dopamine composites exhibited excellent catalytic activities towards both OER and ORR due to its high surface area and 3D hollow architectures. The catalyst showed a low potential (1.720 V *vs*. RHE) at the current density of 10 mA cm^{-2} and small Tafel slope (81 mV dec^{-1}) for OER, meanwhile a high onset-potential (~0.962 V *vs*. RHE) and large diffusion limiting current density (5.55 mA cm^{-2}) for ORR in alkaline media [44].

The bifunctional catalysts to OER and ORR were designed based on the hierarchical carbon-based nanocages to improve the performance of lithium-oxygen batteries. Ir nanoparticles were anchored on the N-doped carbon nanocages with tunable bimodal pore structures. The moderate macropores (~60 nm) combined with the ultrathin mesoporous shells remarkably improved the mass transfer and the infiltration of electrolytes, and the big cavities (~250 nm) of carbon nanocages offered sufficient room to accommodate the Li_2O_2 product, while numerous N-sites and uniformly distributed Ir nanoparticles of 2.3 nm significantly decreased the overpotential. Their synergism endows the Li-O_2 batteries with the high discharge capacity (8,239 mA h g^{-1}), good rate performance, and a small OER-ORR potential gap (0.88 V) [102]. The electrode materials of hierarchical carbon-based nanocages are also promising for zinc-air batteries. With N,S codoped carbon nanocages, the Zn-air batteries exhibited an ORR-OER potential difference of 0.84 V, much lower than 1.07 V for the Pt/C+IrO_2 counterpart, among the top level for the Zn-air batteries to date [43]. The hierarchical Co-N-doped carbon nanocages were constructed by a facile emulsion approach followed by carbonization for Zn-air batteries. The optimal catalyst exhibited a low OER overpotential (420 mV to drive a current density of 10 mA cm^{-2}) and a favorable ORR activity (onset potential of 0.99 V *vs*. RHE), comparable to that of commercial Pt/C and rivals that of Pt/C with better cycling stability. The excellent performance of the catalyst is attributed to the Co-N_x active sites with a high density, high surface area and good conductivity of the materials. More impressively, the assembled rechargeable zinc-air batteries based on the 0.1-Co–NHCs catalyst outperform those afforded by commercial Pt/C, which exhibited a high power density of 239.8 mW cm^{-2}, a small charge-discharge voltage gap (0.84 V@10 mA cm^{-2}) and excellent stability [103].

4.5 Some other advanced catalysts

Fischer-Tropsch synthesis of lower olefins (FTO) is a classical yet modern topic of great significance, which is also the downstream reaction of CO_2 reduction reactions (CO_2RR) with the production of syngas [104,105]. In FTO, the supported Fe-based nanoparticles are the most promising catalysts but suffer from the deterioration of the performances due to the instability of the nanosized active phase of iron carbides. 3D hNCNC is a good platform to construct Fe-based catalyst owing to the tunable nitrogen content in a wide range, high SSA and coexisting micro-meso-macropores for convenient mass transfer. Our mass spectral examinations and theoretical calculations revealed that the Fe-based active phase supported on carbon nanocages experienced a fast size growth in the FTO *via* the iron carbonyl-mediated growth mechanism (Figure 12(a)). Increasing the N-doping content of carbon nanocages can suppress the formation of iron carbonyl and thereby alleviate the growth of Fe-based active phase for FTO, showing exceptional catalytic stability even after 200 h FTO reaction and the highest selectivity for lower olefins up to 54.1% (Figure 12 (b–d)) [41]. Such a strategy could be referential in the catalyst design for the reactions involving metal catalysts and CO reactants.

Featured by the fast mass/charge transport, the mesostructured carbon-based nanocages could be employed as the advanced supports to construct some other efficient catalysts such as CO_2 reduction reactions and nitrogen reduction reactions. The high catalytic performances could be anticipated owing to the unique mesostructures.

5 Conclusions and perspective

Mesostructured carbon-based nanocages not only own the common features of nanocages including perforative hollow interior cavities, high SSA with defective outer surface, tunable electronic structures, excellent electric conductivity and high stability, but also possess the interconnected multiscale pore structure and netlike framework beneficial to mass/charge transportation. In comparison with the ran-

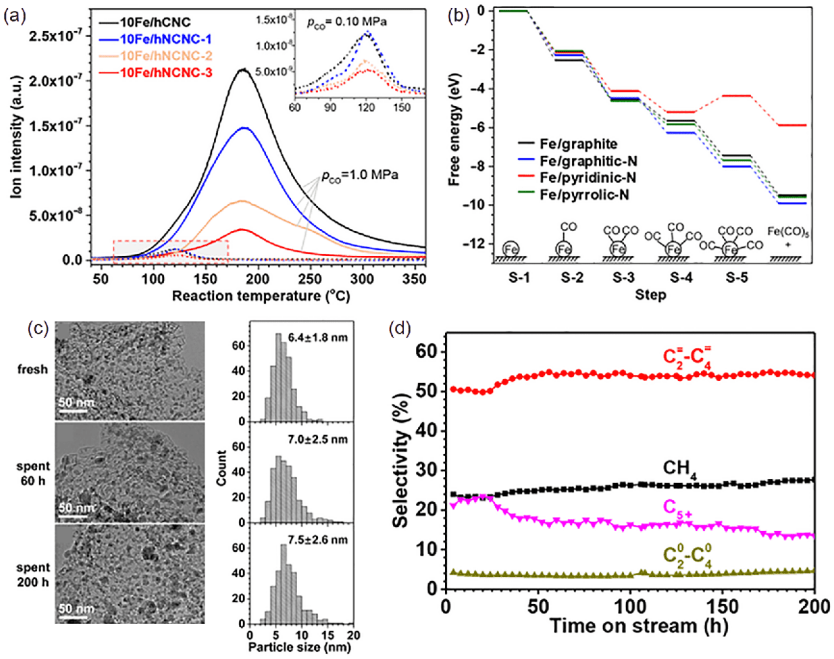

Figure 12 Mechanism and strategy for stabilizing the Fe-based active phase of FTO catalysts and the resulting catalytic performance [41]. (a, b) *In situ* mass spectroscopic examination of iron carbonyls (a) and DFT simulation on its formation *via* the carbonylation of iron species (b). (c, d) Evolutions of morphology and particle size distribution (c) and selectivity (d) of the 35Fe/hNCNC-3 catalyst. Note: The N content in hNCNC-1, -2 and -3 is 3.0 at%, 8.1 at% and 12.0 at%, respectively (color online).

domly-packed nanocages, such hierarchical porous architectures of the mesostructured carbon-based nanocages make them more favorable for promoting the reaction/adsorption-desorption rate, and now become an advanced platform for ECS. In this review, we have summarized the up-to-date progress about the synthesis and energy chemistry applications of mesostructured carbon-based nanocages. The mesostructured carbon-based nanocages and their hybrids with encapsulated or supported foreign species present excellent performances in supercapacitors, rechargeable batteries, and advanced catalysts for energy-related reactions, superior to the nanocages without mesostructures and other nanocarbons. These studies have much enriched the research contents of the field of carbon-based nanomaterials.

Owing to the hollow cavities and porous morphology, usually the density of the mesostructured carbon-based nanocages is quite low (<0.1 g cm^{-3}), which is unfavorable for achieving the high volumetric performances [35]. In addition, the multiscale hierarchical morphology leads to the technique inconvenience to elaborate the electron microscopic observations especially for the encapsulated species and single-site catalysts [10,37,40,68]. In order to better use the mesostructured carbon-based nanocages, there are still many important challenges to be solved. Besides the regulations of structural parameters (*e.g.*, doping configurations, the micropore sizes on the shell) of nanocage building-units and the efficient encapsulating/supporting of foreign species [10], more efforts should be devoted to the morphological and functional moderation of the mesostructures: (1) More mesostructures of carbon-based nanocages with unique functions should be designed and controllably synthesized, which is the basis of further investigations and applications. Keep in mind that they should satisfy the synergic mass/charge transfer for meeting the high-speed energy chemistry process. (2) The correlation between the mesostructures and the ECS performance should be well established. To this end, the multiscale pore structure should be optimized controllably to decrease the surplus mesopores and macropores for achieving higher volumetric performances but without sacrificing the fast mass/charge transfer. Meanwhile, suitable computation methods should be developed to understand the mass/ion/charge transport in the hierarchical architectures, which can provide the guidance to the pore structure regulation. (3) The electrodes of mesostructured carbon-based nanocages with high loading usually have large thicknesses due to their low density, which would impede the ions shuttling and electron transfer. The realization of good performance in commercial electrodes with mass loadings of >10 mg cm^{-2} is highly demanded [3]. (4) Owing to the unique mesostructural characteristics, some new functions and applications could be expected and explored, such as selective adsorption and/or separation of gases/ions, elimination of pollutants in air/water/soil [106–108].

Such efforts could deepen and extend the studies and applications of the mesostructured carbon-based nanocages, and more achievements can be envisaged in the near future.

The idea of constructing mesostructures also provides guidance to improve ECS performance of other materials [109,110].

Acknowledgements This work was supported by the National Key Research and Development Program of China (2017YFA0206500, 2018YFA0209103), and the National Natural Science Foundation of China (21832003, 21773111, 51571110, 21573107).

Conflict of interest The authors declare that they have no conflict of interest.

1 Chu S, Cui Y, Liu N. *Nat Mater*, 2017, 16: 16–22
2 De Luna P, Hahn C, Higgins D, Jaffer SA, Jaramillo TF, Sargent EH. *Science*, 2019, 364: eaav3506
3 Sun H, Zhu J, Baumann D, Peng L, Xu Y, Shakir I, Huang Y, Duan X. *Nat Rev Mater*, 2019, 4: 45–60
4 Pomerantseva E, Bonaccorso F, Feng X, Cui Y, Gogotsi Y. *Science*, 2019, 366: eaan8285
5 Li G, Huang B, Pan Z, Su X, Shao Z, An L. *Energy Environ Sci*, 2019, 12: 2030–2053
6 Kroto HW, Heath JR, O'Brien SC, Curl RF, Smalley RE. *Nature*, 1985, 318: 162–163
7 Iijima S. *Nature*, 1991, 354: 56–58
8 Novoselov KS, Geim AK, Morozov SV, Jiang D, Zhang Y, Dubonos SV, Grigorieva IV, Firsov AA. *Science*, 2004, 306: 666–669
9 Li G, Li Y, Liu H, Guo Y, Li Y, Zhu D. *Chem Commun*, 2010, 46: 3256–3258
10 Wu Q, Yang L, Wang X, Hu Z. *Adv Mater*, 2019, 1904177
11 Tian H, Liang J, Liu J. *Adv Mater*, 2019, 31: 1903886
12 Zhang X, Zhu Y, Bruck AM, Housel LM, Wang L, Quilty CD, Takeuchi KJ, Takeuchi ES, Marschilok AC, Yu G. *Energy Storage Mater*, 2019, 19: 439–445
13 Lyu Z, Xu D, Yang L, Che R, Feng R, Zhao J, Li Y, Wu Q, Wang X, Hu Z. *Nano Energy*, 2015, 12: 657–665
14 Service RF. *Science*, 2012, 335: 1167–1168
15 Hemminger J, Crabtree G, Sarrao J. From quanta to the continuum: opportunities for mesoscale science. A report from the Basic Energy Science Advisory Committee. US: Department of Energy, 2012
16 Lang X, Hirata A, Fujita T, Chen M. *Nat Nanotech*, 2011, 6: 232–236
17 Lu Q, Lattanzi MW, Chen Y, Kou X, Li W, Fan X, Unruh KM, Chen JG, Xiao JQ. *Angew Chem Int Ed*, 2011, 50: 6847–6850
18 Parlett CMA, Wilson K, Lee AF. *Chem Soc Rev*, 2013, 42: 3876–3893
19 Shi H, Fang Z, Zhang X, Li F, Tang Y, Zhou Y, Wu P, Yu G. *Nano Lett*, 2018, 18: 3193–3198
20 Wu Q, Yang L, Wang X, Hu Z. *Acc Chem Res*, 2017, 50: 435–444
21 Ugarte D. *Nature*, 1992, 359: 707–709
22 Kroto HW. *Nature*, 1992, 359: 670–671
23 Saito Y, Yoshikawa T, Okuda M, Ohkohchi M, Ando Y, Kasuya A, Nishina Y. *Chem Phys Lett*, 1993, 209: 72–76
24 Saito Y, Yoshikawa T, Okuda M, Fujimoto N, Sumiyama K, Suzuki K, Kasuya A, Nishina Y. *J Phys Chem Solids*, 1993, 54: 1849–1860
25 Yosida Y, Shida S, Ohsuna T, Shiraga N. *J Appl Phys*, 1994, 76: 4533–4539
26 Seraphin S, Zhou D, Jiao J. *J Appl Phys*, 1996, 80: 2097–2104
27 Messina G, Santangelo S. *Carbon, the Future Material for Advanced Technology Applications*. In: Ascheron CE, Koelsch HJ, Duhm AH, Eds. Topics in Applied Physics. Volume 100. Berlin Heidelberg: Springer-Verlag, 2006. 187–216
28 Jang J, Lim B. *Adv Mater*, 2002, 14: 1390–1393
29 Lee KT, Jung YS, Oh SM. *J Am Chem Soc*, 2003, 125: 5652–5653
30 Chai GS, Yoon SB, Kim JH, Yu JS. *Chem Commun*, 2004, 23: 2766–2767
31 Wang XZ, Qian MJ, Xiao P, Jiang XF, Jian GQ, Hu Z. Chinese Patent. ZL200810023448.X. 2010-02-03
32 Xie K, Qin X, Wang X, Wang Y, Tao H, Wu Q, Yang L, Hu Z. *Adv Mater*, 2012, 24: 347–352
33 Chen S, Bi J, Zhao Y, Yang L, Zhang C, Ma Y, Wu Q, Wang X, Hu Z. *Adv Mater*, 2012, 24: 5593–5597
34 Zhao J, Lai H, Lyu Z, Jiang Y, Xie K, Wang X, Wu Q, Yang L, Jin Z, Ma Y, Liu J, Hu Z. *Adv Mater*, 2015, 27: 3541–3545
35 Bu Y, Sun T, Cai Y, Du L, Zhuo O, Yang L, Wu Q, Wang X, Hu Z. *Adv Mater*, 2017, 29: 1700470
36 Du L, Wu Q, Yang L, Wang X, Che R, Lyu Z, Chen W, Wang X, Hu Z. *Nano Energy*, 2019, 57: 34–40
37 Shen L, Sun T, Zhuo O, Che R, Li D, Ji Y, Bu Y, Wu Q, Yang L, Chen Q, Wang X, Hu Z. *ACS Appl Mater Interfaces*, 2016, 8: 16664–16669
38 Jiang Y, Yang L, Sun T, Zhao J, Lyu Z, Zhuo O, Wang X, Wu Q, Ma J, Hu Z. *ACS Catal*, 2015, 5: 6707–6712
39 Zhang Z, Wu Q, Mao K, Chen Y, Du L, Bu Y, Zhuo O, Yang L, Wang X, Hu Z. *ACS Catal*, 2018, 8: 8477–8483
40 Zhang Z, Chen Y, Zhou L, Chen C, Han Z, Zhang B, Wu Q, Yang L, Du L, Bu Y, Wang P, Wang X, Yang H, Hu Z. *Nat Commun*, 2019, 10: 1657
41 Zhuo O, Yang L, Gao F, Xu B, Wu Q, Fan Y, Zhang Y, Jiang Y, Huang R, Wang X, Hu Z. *Chem Sci*, 2019, 10: 6083–6090
42 Du L, Cheng X, Gao F, Li Y, Bu Y, Zhang Z, Wu Q, Yang L, Wang X, Hu Z. *Chem Commun*, 2019, 55: 6365–6368
43 Fan H, Wang Y, Gao F, Yang L, Liu M, Du X, Wang P, Yang L, Wu Q, Wang X, Hu Z. *J Energy Chem*, 2019, 34: 64–71
44 Cai S, Meng Z, Tang H, Wang Y, Tsiakaras P. *Appl Catal B-Environ*, 2017, 217: 477–484
45 Woo SW, Dokko K, Sasajima K, Takei T, Kanamura K. *Chem Commun*, 2006, 4099–4101
46 Chen M, Su Z, Jiang K, Pan Y, Zhang Y, Long D. *J Mater Chem A*, 2019, 7: 6250–6258
47 Chen Z, Ye S, Evans SD, Ge Y, Zhu Z, Tu Y, Yang X. *Small*, 2018, 14: 1704015
48 Zhang R, Hummelgård M, Olin H. *Carbon*, 2010, 48: 424–430
49 Zhang H, Gai P, Cheng R, Wu L, Zhang X, Chen J. *Anal Methods*, 2013, 5: 3591–3600
50 Zhang J, Yang CP, Yin YX, Wan LJ, Guo YG. *Adv Mater*, 2016, 28: 9539–9544
51 Wang X, Li Y, Du L, Gao F, Wu Q, Yang L, Chen Q, Wang X, Hu Z. *Acta Chim Sin*, 2018, 76: 627–632
52 Zhang H, Cao G, Yang Y. *Energy Environ Sci*, 2009, 2: 932–943
53 Sun Y, Wu Q, Shi G. *Energy Environ Sci*, 2011, 4: 1113–1132
54 Liu J, Wang X, Gao J, Zhang Y, Lu Q, Liu M. *Electrochim Acta*, 2016, 211: 183–192
55 Shao J, Song M, Wu G, Zhou Y, Wan J, Ren X, Ma F. *Energy Storage Mater*, 2018, 13: 57–65
56 Wu ZS, Parvez K, Feng X, Müllen K. *Nat Commun*, 2013, 4: 2487
57 Zhao J, Jiang Y, Fan H, Liu M, Zhuo O, Wang X, Wu Q, Yang L, Ma Y, Hu Z. *Adv Mater*, 2017, 29: 1604569
58 Yang X, Cheng C, Wang Y, Qiu L, Li D. *Science*, 2013, 341: 534–537
59 Xu Y, Lin Z, Zhong X, Huang X, Weiss NO, Huang Y, Duan X. *Nat Commun*, 2014, 5: 4554
60 Ma Q, Yao Y, Yan M, Zhao J, Ge C, Wu Q, Yang L, Wang X, Hu Z. *Sci China Mater*, 2019, 62: 1393–1402
61 Zhang G, Ren L, Hu D, Zhang S, Gu H. *J Alloys Compd*, 2019, 781: 407–414
62 Lin TW, Hsiao MC, Wang AY, Lin JY. *ChemElectroChem*, 2017, 4: 620–627
63 Lyu Z, Yang L, Xu D, Zhao J, Lai H, Jiang Y, Wu Q, Li Y, Wang X, Hu Z. *Nano Res*, 2015, 8: 3535–3543
64 Zang J, Chen JJ, Zhang CL, Qian H, Zheng MS, Dong QF. *J Mater Chem A*, 2014, 2: 6343–6347

65 Zhang S, Wang G, Zhang Z, Wang B, Bai J, Wang H. *Small*, 2019, 15: 1900565
66 Zeng X, Ding Z, Ma C, Wu L, Liu J, Chen L, Ivey DG, Wei W. *ACS Appl Mater Interfaces*, 2016, 8: 18841–18848
67 Liu M, Fan H, Zhuo O, Du X, Yang L, Wang P, Yang L, Wu Q, Wang X, Hu Z. *Chem Eur J*, 2019, 25: 3843–3848
68 Liu M, Fan H, Zhuo O, Chen J, Wu Q, Yang L, Peng L, Wang X, Che R, Hu Z. *Nano Energy*, 2020, 68: 104368
69 Wang N, Bai Z, Fang Z, Zhang X, Xu X, Du Y, Liu L, Dou S, Yu G. *ACS Mater Lett*, 2019, 1: 265–271
70 Seh ZW, Sun Y, Zhang Q, Cui Y. *Chem Soc Rev*, 2016, 45: 5605–5634
71 Li Z, Wu HB, Lou (David) XW. *Energy Environ Sci*, 2016, 9: 3061–3070
72 Jayaprakash N, Shen J, Moganty SS, Corona A, Archer LA. *Angew Chem Int Ed*, 2011, 50: 5904–5908
73 Zhu X, Ye J, Lu Y, Jia X. *ACS Sustain Chem Eng*, 2019, 7: 11241–11249
74 Cai J, Zhang Z, Yang S, Min Y, Yang G, Zhang K. *Electrochim Acta*, 2019, 295: 900–909
75 Ma Z, Jing F, Fan Y, Li J, Zhao Y, Shao G. *J Alloys Compd*, 2019, 789: 71–79
76 Liu T, Dai C, Jia M, Liu D, Bao SJ, Jiang J, Xu M, Li CM. *ACS Appl Mater Interfaces*, 2016, 8: 16063–16070
77 Lu YC, Gallant BM, Kwabi DG, Harding JR, Mitchell RR, Whittingham MS, Shao-Horn Y. *Energy Environ Sci*, 2013, 6: 750–768
78 Zhao C, Yu C, Liu S, Yang J, Fan X, Huang H, Qiu J. *Adv Funct Mater*, 2015, 25: 6913–6920
79 Wang L, Lyu Z, Gong L, Zhang J, Wu Q, Wang X, Huo F, Huang W, Hu Z, Chen W. *ChemNanoMat*, 2017, 3: 415–419
80 Jiang X, Wang X, Shen L, Wu Q, Wang Y, Ma Y, Wang X, Hu Z. *Chin J Catal*, 2016, 37: 1149–1155
81 Fan H, Mao K, Liu M, Zhuo O, Zhao J, Sun T, Jiang Y, Du X, Zhang X, Wu Q, Che R, Yang L, Wu Q, Wang X, Hu Z. *J Mater Chem A*, 2018, 6: 21313–21319
82 Shao M, Chang Q, Dodelet JP, Chenitz R. *Chem Rev*, 2016, 116: 3594–3657
83 Wang YJ, Zhao N, Fang B, Li H, Bi XT, Wang H. *Chem Rev*, 2015, 115: 3433–3467
84 Gasteiger HA, Marković NM. *Science*, 2009, 324: 48–49
85 Fang B, Kim JH, Kim M, Kim M, Yu JS. *Phys Chem Chem Phys*, 2009, 11: 1380–1387
86 Jiang L, Mi L, Wang K, Wu Y, Li Y, Liu A, Zhang Y, Hu Z, Liu S. *ACS Appl Mater Interfaces*, 2017, 9: 31968–31976
87 Sun T, Wu Q, Che R, Bu Y, Jiang Y, Li Y, Yang L, Wang X, Hu Z. *ACS Catal*, 2015, 5: 1857–1862
88 Sun T, Wu Q, Zhuo O, Jiang Y, Bu Y, Yang L, Wang X, Hu Z. *Nanoscale*, 2016, 8: 8480–8485
89 Gong K, Du F, Xia Z, Durstock M, Dai L. *Science*, 2009, 323: 760–764
90 Dai LM. *Carbon-Based Metal-Free Catalysts: Design and Applications*. Weinheim: Wiley-VCH, 2018
91 Yang L, Shui J, Du L, Shao Y, Liu J, Dai L, Hu Z. *Adv Mater*, 2019, 31: 1804799
92 Yang L, Jiang S, Zhao Y, Zhu L, Chen S, Wang X, Wu Q, Ma J, Ma Y, Hu Z. *Angew Chem Int Ed*, 2011, 50: 7132–7135
93 Wu Z, Liu R, Wang J, Zhu J, Xiao W, Xuan C, Lei W, Wang D. *Nanoscale*, 2016, 8: 19086–19092
94 Zhu J, Zhou H, Zhang C, Zhang J, Mu S. *Nanoscale*, 2017, 9: 13257–13263
95 Jia Y, Zhang L, Zhuang L, Liu H, Yan X, Wang X, Liu J, Wang J, Zheng Y, Xiao Z, Taran E, Chen J, Yang D, Zhu Z, Wang S, Dai L, Yao X. *Nat Catal*, 2019, 2: 688–695
96 Zhang J, Ma L, Gan M, Yang F, Fu S, Li X. *J Power Sources*, 2015, 288: 42–52
97 Peng Y, Lu B, Chen S. *Adv Mater*, 2018, 30: 1801995
98 Zhang L, Doyle-Davis K, Sun X. *Energy Environ Sci*, 2019, 12: 492–517
99 Wu J, Xiong L, Zhao B, Liu M, Huang L. *Small Methods*, 2020, 4: 1900540
100 Jia N, Weng Q, Shi Y, Shi X, Chen X, Chen P, An Z, Chen Y. *Nano Res*, 2018, 11: 1905–1916
101 Lu Z, Wang J, Huang S, Hou Y, Li Y, Zhao Y, Mu S, Zhang J, Zhao Y. *Nano Energy*, 2017, 42: 334–340
102 Shen J, Wu H, Sun W, Qiao J, Cai H, Wang Z, Sun K. *Chem Eng J*, 2019, 358: 340–350
103 Chen S, Cheng J, Ma L, Zhou S, Xu X, Zhi C, Zhang W, Zhi L, Zapien JA. *Nanoscale*, 2018, 10: 10412–10419
104 Torres Galvis HM, Bitter JH, Khare CB, Ruitenbeek M, Dugulan AI, de Jong KP. *Science*, 2012, 335: 835–838
105 Ross MB, Dinh CT, Li Y, Kim D, De Luna P, Sargent EH, Yang P. *J Am Chem Soc*, 2017, 139: 9359–9363
106 Yang Y, Yang X, Liang L, Gao Y, Cheng H, Li X, Zou M, Ma R, Yuan Q, Duan X. *Science*, 2019, 364: 1057–1062
107 Xu J, Liu C, Hsu PC, Zhao J, Wu T, Tang J, Liu K, Cui Y. *Nat Commun*, 2019, 10: 2440
108 Wan S, Wan H, Bi H, Zhu J, He L, Yin K, Su S, Sun L. *Nanoscale*, 2018, 10: 17015–17020
109 Lai H, Wu Q, Zhao J, Shang L, Li H, Che R, Lyu Z, Xiong J, Yang L, Wang X, Hu Z. *Energy Environ Sci*, 2016, 9: 2053–2060
110 Shang L, Li H, Lai H, Li D, Wu Q, Yang L, Wang X, Hu Z. *J Power Sources*, 2016, 326: 279–284